# GAS-DISPLACEMENT OF VISCOELASTIC LIQUIDS IN CAPILLARY TUBES

**Erick Fabrízio Quintella**
Department of Mechanical Engineering, Pontifícia Universidade Católica do Rio de Janeiro, Rua Marquês de São Vicente 225, Gávea, Rio de Janeiro, RJ, 22453-900, Brasil, erick@mec.puc-rio.br

**Paulo Roberto Souza Mendes**
Department of Mechanical Engineering, Pontifícia Universidade Católica do Rio de Janeiro, Rua Marquês de São Vicente 225, Gávea, Rio de Janeiro, RJ, 22453-900, Brasil, pmendes@mec.puc-rio.br

**Márcio da Silveira Carvalho**
Department of Mechanical Engineering, Pontifícia Universidade Católica do Rio de Janeiro, Rua Marquês de São Vicente 225, Gávea, Rio de Janeiro, RJ, 22453-900, Brasil, msc@mec.puc-rio.br

***Abstract.*** *Displacement of a liquid in a capillary tube by gas injection occurs in many situations, like enhanced oil recovery, coating of catalytic converters and gas-assisted injection molding. Generally the liquid being displaced is a polymeric solution or dispersion, which is not Newtonian. Viscoelastic forces alter the force balance in various parts of the flow and consequently change the amount of liquid left attached to the capillary wall. Models of such flows must rely on theories that can account for the different behavior of microstructured liquids in shear and extensional flow. Moreover, displacement flows involve a free surface, and the domain where the differential equations are posed is unknown a priori being part of the solution. These two characteristics make the problem extremely complex. Here, the two-dimensional free surface flow near the gas-liquid interface was modeled using one differential constitutive equation that approximates viscoelastic behavior of dilute polymer solutions, namely Oldroyd-B, together with momentum and continuity equations. The equation system was solved with the Finite Element Method. The resulting non-linear system of algebraic equations was solved by Newton's method. The results show the effect of the viscoelastic character of the liquid on the free surface shape and the film thickness attached to the capillary wall.*

***Keywords:*** *Free surface flow, two-phase viscoelastic flow, gas-assisted injection molding, gas-liquid interface, elastic dumbbell models.*

## 1. INTRODUCTION

The displacement of a liquid inside small passages and capillary tubes by another liquid or gas occurs in many practical situations. The most important examples are the flow inside the porous space in enhanced oil recovery methods, coating process of catalytic converter and inside tubes and gas assisted injection molding. These flows belong to a class of flows generally referred to as free surface flows; the configuration and position of the interface between the two fluids is unknown a priori and is part of the solution of the problem.

Figure 1 shows the region close to the tip of the interface of a liquid being displaced by a gas.

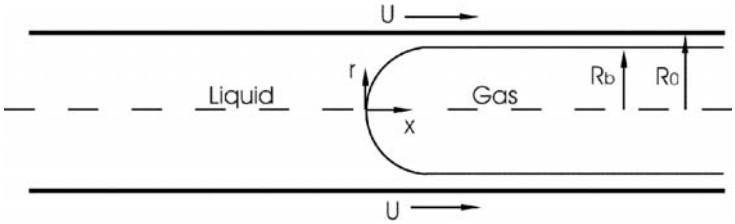

Figure 1. Sketch of a liquid-displacement problem.

Since the frame of reference is attached to the bubble tip, all happens as if the tube wall is moving with the bubble speed $U$ in the opposite direction. A certain amount of liquid remains attached to the capillary wall, as shown in the figure. The more liquid is left on the wall the least efficient is the displacement process. This information is one of the main goals of theoretical and experimental analysis of displacement flows. A dimensionless measurement of the thickness of the liquid film attached to the wall used in the literature is the fraction coverage $m$, defined as the fraction of the tube cross-sectional area coated with liquid after bubble penetration, i.e.

$$m = \frac{R_0^2 - R_b^2}{R_0^2}, \tag{1}$$

where $R_0$ is the tube radius and $R_b$ is the radius of the penetrating bubble. In some of the situations described, the liquid being displaced is a polymeric solution or dispersion and is non-Newtonian. Viscoelastic forces near the interface changes the force balance in that region and consequently the configuration of the free surface and the fractional coverage. The two important dimensionless groups in the displacement of viscoelastic liquids in capillary tubes, our case of interest, are the capillary number $Ca$, which is the ratio of viscous to surface tension forces, and the Deborah number $De$, which is the ratio between a relaxation time characteristic of the liquid and a characteristic time of the deformation process:

$$Ca = \frac{\eta_0 U}{\sigma}, \qquad De = \lambda \dot{\gamma}_w. \tag{2}$$

Here $\eta_0$ is the solvent viscosity, $U$ is the bubble velocity, σ is the interfacial tension between the inviscid penetrating gas and the displaced liquid, $\lambda$ is a relaxation time characteristic of the liquid and $\dot{\gamma}_w = 2U/R_0$ is the (Newtonian) shear rate at the wall, assumed to be characteristic of the process.

Different analyses on displacement of liquids in capillary tubes have been performed for Newtonian as well as for viscoelastic liquids, and a brief summary of these results is given in the following paragraphs.

The first experimental study of a long gas bubble penetrating through a liquid was performed by Fairbrother and Stubbs (1935), who studied the penetration of an air bubble through a Newtonian liquid in a circular tube. Their most important result is the proposition of a direct relation between the fractional coverage $m$ with the capillary number $Ca$, given by $m = Ca^{1/2}$.

Another classical work on liquid displacement in capillary tubes was developed by Bretherton (1960). He studied the motion of long air bubbles in capillary tubes filled with Newtonian viscous liquids. Bretherton assumed zero shear stress at the interface, as well as small capillary numbers. Bretherton performed experimental tests with tubes of diameters small enough to neglect gravity effects. His theoretical analysis showed that the velocity of the interface $U$ exceeds the mean flow velocity by a value of $WU$, where $W = 1.29(3Ca)^{2/3}$. Bretherton obtained $W$ studying only the frontal and transition regions of the bubble. In a first approximation, he considered a planar flow at the region far from the bubble ends. Later he included curvature effects in the equations, obtaining results similar to the first approximation with a maximum error of 10%. The author compared some

of his experimental results with theoretical predictions for $W$. A good agreement is observed between both experimental e theoretical data, mainly at the high capillary number range studied.

In the same year, Taylor (1960) published a work where he developed an experimental study on removal of Newtonian liquids from capillary tubes through gas injection. The main objective was to determinate the amount of liquid deposited on the tube wall during flow. Taylor showed the dependence of the fractional coverage $m$, with the capillary number, $Ca$. The plot suggests a limit value for $m$ corresponding to approximately 0.56 when $Ca$ tends to 2. Fairbrother and Stubbs had already proposed a direct relation of $m$ with the capillary number, as mentioned. Taylor compared his experimental results with the empirical equation proposed by Fairbrother and Stubbs (1935) and verified that their relation is only valid for a narrow capillary number range of $0 < Ca < 0.09$. Without making any visualization experiment, Taylor suggested three possible patterns for the streamlines relative to a frame of reference attached to the bubble tip. For small capillary numbers the flow would present reversions with points and rings of stagnation. Increasing the capillary number would decrease the reverse flow, allowing the existence of only one stagnation point.

Two years later, Cox (1962) published the continuation of the experiments initiated by Taylor and concluded that the fraction of mass deposited at the wall reaches an asymptotic value of 0.60 when $Ca$ tends to 10. Cox also developed a simplified theoretical analysis to calculate $m$. His analysis appears to fit in the cases where surface tension forces can be neglected in view of viscous forces ($Ca >> 1$). The investigation about the streamline patterns proposed by Taylor is performed by Cox (1964) through a visualization experiment. Cox confirmed the patterns for extreme values of the capillary number ($Ca >> 1$ and $Ca << 1$), but the transition pattern could not be confirmed. Still, the author showed the important conclusion that the bubble interface disturbs only the regions in its vicinity, being this disturbance approximately 1.5 times the tube diameter.

Having summarized the classical works on displacement of Newtonian liquids by gas injection, we present some relevant results for a similar problem, but now displacing a viscoelastic liquid.

Ro and Homsy (1995) presented a theoretical study about the effect of elasticity on the meniscus shape and on film thickness for the flow induced by a long air bubble steadily displacing a polymeric liquid confined by two parallel plates, i.e. Hele-Shaw flow. The authors sought asymptotic solutions by perturbation expansions to solve the problem, and the assumptions were that the displaced viscoelastic liquid wets the wall and that both capillary number and local Weissenberg number $We$, a measure of the elasticity of the flow, were small. The Oldroyd-B constitutive equation was used to model the viscoelastic liquid and the authors stressed that the transition region between the advancing meniscus and the entrained film is where the liquid rheology has its greatest effect. According to their analysis, as the liquid becomes more viscoelastic, the film thickness decreases and the pressure drop at the meniscus tip increases. A detailed analysis of their work allows concluding that the dominant mechanisms are the resistance to stream-wise strain, tending to lower the film thickness, and the buildup of shear stress, tending to raise the film thickness.

Huzyak and Koelling (1997) performed experimental investigations of penetration of a long bubble through a viscoelastic liquid in a capillary tube. The main goal was to identify the effects of liquid elasticity on the thickness of the liquid film attached to the wall. Experiments were performed with four test liquids including two Newtonian and two Boger liquids (highly elastic liquids showing constant shear viscosities). The authors obtained results for the fractional coverage $m$, as a function of capillary number and Deborah number, $De$. Deborah number measures the deviation of elastic fluids from Newtonian behavior. The authors observed that for small Deborah number, $De < 1$, both viscoelastic liquids exhibit a fractional coverage identical to that of a Newtonian liquid at an equivalent capillary number. The fractional coverage for both viscoelastic liquids begins to increase relative to the Newtonian result at $De \approx 1$. Fractional coverage continues to increase with Deborah number for all $De \geq 1$. At $De \approx 5$ fractional coverage is 30% greater than the Newtonian liquid result. They also found that the fractional coverage depend on the tube diameter for the viscoelastic liquids. It is important to point out that the experimental results of Huzyak and Koelling (1997) showed the opposite trend of the theoretical analysis of Ro and Homsy (1995).

Another important study dealing with viscoelastic free surface flows was recently presented by Lee et al. (2002). They applied a finite element formulation to study the effect of viscoelasticity on free surface flows, analyzing both a Hele-Shaw flow and the slot coating of viscoelastic liquids. The viscoelastic liquids were modeled by means of three distinct differential constitutive equations: the Oldroyd-B, FENE-CR and FENE-P models. The calculation showed the formation of an elastic stress boundary layer in the region adjacent to the interface, and the polymeric stresses associated to this boundary layer is found to be responsible for changes in the meniscus shape as well as the thickness variation of the film of liquid attached to the solid plates.

The goal of this work is to analyze the effect of the viscoelastic character of the displaced liquid on the free surface shape and on the film thickness attached to the capillary wall, by solving the momentum and continuity equations coupled with the Oldroyd-B model to describe the mechanical behavior of the flowing liquid.

## 2. MATHEMATICAL FORMULATION

This section describes the governing equations, the constitutive model and boundary conditions for the situation studied here.

### 2.1. Governing Equations

The two-dimensional, steady free surface flow of the displaced liquid in a capillary tube is described by the equations that impose conservation of mass and momentum:

$$\nabla . \underline{u} = 0 , \tag{3}$$

$$0 = -\nabla p + \nabla . \underline{\underline{\tau}} , \tag{4}$$

where $\underline{u}$ is the velocity vector, $p$ is the pressure and $\underline{\underline{\tau}}$ is the extra-stress tensor. It is clear from Eq. (4) that inertial effects are neglected in our model. The governing equations are solved by considering a coordinate system attached to the bubble tip.

### 2.2. Constitutive Equation

To analyze the physics of polymer stretching as well as to determine the flow field modification due to a diluted polymer solution in the displacement of viscoelastic liquids in capillary tubes, we choose the Oldroyd-B differential constitutive equation (Bird et al. (1987)), written below in tensor notation:

$$\begin{aligned} &\underline{\underline{\tau}} = \underline{\underline{\tau}}_s + \underline{\underline{\tau}}_p , \\ &\underline{\underline{\tau}}_s = \eta_s \underline{\underline{\dot{\gamma}}}, \\ &\underline{\underline{\tau}}_p + \lambda \left\{ \underline{u} . \nabla \underline{\underline{\tau}}_p - \left[ \left( \underline{\underline{\tau}}_p . \nabla \underline{u} \right)^T + \left( \underline{\underline{\tau}}_p . \nabla \underline{u} \right) \right] \right\} = \eta_p \underline{\underline{\dot{\gamma}}} . \end{aligned} \tag{5}$$

Here, the extra-stress tensor is split in a Newtonian solvent stress $\underline{\underline{\tau}}_s$, and a polymer stress $\underline{\underline{\tau}}_p$. The solvent and polymer contribution to the shear viscosity are denoted, respectively, by $\eta_s$ and $\eta_p$. The rate-of-deformation tensor is denoted by $\underline{\underline{\dot{\gamma}}}$ and $\lambda$ is the relaxation time of the liquid.

### 2.3. Boundary Conditions

The boundary conditions applied on the free surface are:

- kinematic condition

$$\underline{n}.\underline{u} = 0\,; \tag{6}$$

- stress balance

$$\underline{n}.\left(\underline{\underline{\tau}} - p\underline{\underline{I}}\right) = \frac{\sigma}{R_m}\underline{n}\,; \tag{7}$$

Additional boundary conditions are stated below:

- non-slip condition on the tube wall

$$\underline{u} = U\underline{e}_x\,; \tag{8}$$

- symmetry condition at the centerline

$$\underline{n}.\underline{u} = 0 \quad , \quad \underline{t}.\underline{\underline{T}}.\underline{n} = 0\,; \tag{9}$$

- fully developed flow with pressure free at the outflow

$$\underline{n}.\nabla\underline{u} = 0\,; \tag{10}$$

- fully developed flow with pressure imposed at the inflow

$$\underline{n}.\nabla\underline{u} = 0 \quad , \quad p = P_0\,. \tag{11}$$

In these equations, $\underline{n}$ and $\underline{t}$ are the unit vectors normal and tangent to the domain boundary, respectively. $\underline{\underline{T}}$ is the total stress tensor, $\underline{e}_x$ is the unit vector in the axial direction, $U$ is the velocity at the tube wall, $P_0$ is the imposed pressure at the inflow, σ is the surface tension and $R_m$ is the local mean radius of curvature of the interface.

Boundary conditions for the Oldroyd-B constitutive equation are necessary only at the inflow. Accepting the suggestion of Pasquali and Scriven (2002), we preferred to neglect the polymeric stress convective term at the inflow:

- neglect polymeric stress convective term at the inflow

$$\underline{u}.\nabla\underline{\underline{\tau}}_p = 0\,. \tag{12}$$

## 3. NUMERICAL APPROACH

A finite element formulation is applied to study the displacement of viscoelastic liquids in capillary tubes. The solution method implemented is the DEVSS-G/SUPG formulation proposed by Guenette and Fortin (1995) and Brooks and Hughes (1982).

### 3.1. Free Surface Parametrization

The relevant differential equations are posed in an unknown domain; the position of the liquid free surface is part of the solution. A simple way of solving this type of problem is to use a Picard iteration, i.e. solve the flow and the domain position separately. This procedure is not very efficient and in most cases the iteration does not converge. To compute a free boundary problem in a more efficient way, the set of differential equations posed in the unknown physical domain has to be transformed to an equivalent set defined in a known reference domain, usually called computational domain. This transformation is made by a mapping $\underline{x} = \underline{x}(\underline{\xi})$ that connects the two domains. The inverse of the mapping that minimizes the functional is governed by elliptic differential equations identical to those encountered in diffusion transport with variable diffusion coefficients. The coordinates of the reference domain satisfy

$$\nabla.\left(\underline{\underline{\mathfrak{D}}}\nabla\underline{\xi}\right) = 0\,, \tag{13}$$

where $\underline{\underline{\mathfrak{D}}}$ is the diffusion coefficient tensor and $\underline{\xi}$ are the coordinates of the reference domain.

Boundary conditions are needed to solve the second-order partial differential equations (13). Along solid walls and synthetic inlet and outlet planes, the boundary is located by imposing a relation between the physical coordinates $x$ and $r$ from the equation that describes the shape of the boundary, and stretching functions are used to distribute the points along the boundaries. The free boundary (gas-liquid interface) is located by imposing the kinematic condition (Eq. (6)). The discrete versions of the mapping equations are generally referred to as mesh generation equations.

### 3.2. Interpolation Functions

The unknown fields are written as a linear combination of Lagrange polynomial basis functions. Thus, the velocity vector $\underline{u}$, pressure $p$, nodal position vector $\underline{x}$, interpolated velocity gradient tensor $\underline{\underline{g}}$ and polymeric stress tensor $\underline{\underline{\tau}}_p$ are approximated by, respectively:

$$\underline{u} = \sum_{j=1}^{9}\left(\underline{U}_j \phi_j\right), \quad p = \sum_{j=1}^{3}\left(P_j \chi_j\right), \quad \underline{x} = \sum_{j=1}^{9}\left(\underline{X}_j \phi_j\right), \quad \underline{\underline{g}} = \sum_{j=1}^{4}\left(\underline{\underline{G}}_j \psi_j\right), \quad \underline{\underline{\tau}}_p = \sum_{j=1}^{9}\left(\underline{\underline{\mathrm{I}}}_{pj} \psi_j\right). \tag{14}$$

Here, $\underline{U}_j, P_j, \underline{X}_j, \underline{\underline{G}}_j, \underline{\underline{\mathrm{I}}}_{pj}$ are the basis functions coefficients, and represent the unknowns of the discretized problem. The basis functions $\phi_j(\xi,\eta)$ are biquadratic, $\chi_j(\xi,\eta)$ are linear discontinuous and $\psi_j(\xi,\eta)$ are bilinear, all chosen to satisfy the Babüska-Brezzi condition.

### 3.3. Weak Formulation of the Governing Equations in the Reference Domain

The conservation of mass, conservation of linear momentum, interpolated velocity gradient and mesh generation equations are solved using the Galerkin method. For its hyperbolic nature, the Oldroyd-B differential constitutive equation is solved using the Petrov-Galerkin streamline upwinding method (SUPG). The weak forms of the governing equations are, in tensor notation:

- Conservation of mass

$$R_c = \int_{\Omega} (\nabla . \underline{u}) \chi J d\Omega \tag{15}$$

- Conservation of linear momentum

$$R_m = \int_{\Omega} tr\left(\underline{\underline{T}} . \nabla \underline{w}\right) J d\Omega - \int_{\Gamma} \left(\underline{n} . \underline{\underline{T}}\right) \underline{w} J d\Gamma \tag{16}$$

- Interpolated velocity gradient

$$R_g = \int_{\Omega} \left( \underline{\underline{g}} - \nabla \underline{u} + \frac{\nabla . \underline{u}}{tr \underline{\underline{I}}} \underline{\underline{I}} \right) : \underline{\underline{\psi}} J d\Omega \tag{17}$$

- Mesh generation

$$R_X = -\int_{\Omega} \left(\nabla \underline{w} . \underline{\underline{\mathfrak{D}}} . \nabla \underline{\xi}\right) J d\Omega + \int_{\Gamma} \left(\underline{n} . \underline{\underline{\mathfrak{D}}} . \nabla \underline{\xi}\right) \underline{w} d\Gamma \tag{18}$$

- Oldroyd-B constitutive model

$$R\tau_p = \int_{\Omega} \left\{ \underline{\underline{\tau}}_p + \lambda \left[ \underline{u} . \nabla \underline{\underline{\tau}}_p - \left( \underline{\underline{\tau}}_p . \nabla \underline{u} \right)^T - \left( \underline{\underline{\tau}}_p . \nabla \underline{u} \right) \right] - \eta_p \dot{\underline{\underline{\gamma}}} \right\} : \underline{\underline{\varphi}} J d\Omega \tag{19}$$

Here, $\Omega$ and $\Gamma$ denote the reference domain and its boundary, respectively. $J$ is the Jacobian of the mapping between the physical and reference domain, $\chi$ is the scalar weighting function for the conservation of mass equation, $\underline{w}$ is the vector weighting function for the conservation of momentum and mesh generation equations, $\underline{\underline{\psi}}$ is the tensor weighting function for the interpolated

velocity gradient, $\underline{\underline{\varphi}}$ is the tensor weighting function for the Oldroyd-B constitutive equation and $\underline{\underline{I}}$ is the unit tensor.

### 3.4. Solution of the Problem via Newton Iterations

The resulting nonlinear system of equations is solved by the Newton's method:

$$\underline{\underline{J}}.\delta\underline{c} = -\underline{R}(\underline{c}), \tag{20}$$

$$\underline{c}^{k+1} = \underline{c}^{k} + \delta\underline{c}\,. \tag{21}$$

$\underline{\underline{J}}$ is the Jacobian matrix containing the derivatives of all equations with respect to all unknowns, $\underline{c}$ is the solution vector containing all the unknowns of the problem, $\delta\underline{c}$ is the increment in the solution vector, $\underline{R}$ is a vector of weighted residuals and $k$ indicates the present iteration.

## 4. RESULTS

### 4.1. Newtonian Results

Before presenting the analysis of the displacement of viscoelastic liquids in capillary tubes, some classical results for Newtonian liquids are presented in order to test the solution procedure, provide basic information on the subject and gain insight for more complex analysis later.

Figure (2) shows the dependence of the liquid film thickness deposited at the tube wall on the capillary number. Simulations cover a capillary number range of $0.01 \leq Ca \leq 10$. Besides theoretical predictions obtained in the present work, we reproduce the experimental data obtained by Taylor (1960). The agreement between both results is excellent. The result obtained by Cox (1962), which suggests a constant value of 0.6 to the fractional coverage for capillary number above 10, is also confirmed. The experimental results obtained by Taylor, as well as the theoretical predictions of the present work, show that for a given viscosity and a given surface tension the film thickness deposited at the wall is controlled by the velocity of the interface. Therefore, processes whose objective is to obtain a thin film thickness must be performed at low flow rates.

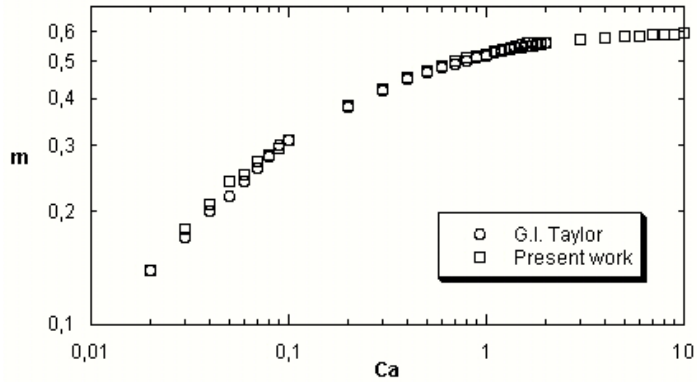


Figure 2. Newtonian liquid film thickness as a function of *Ca*.

Taylor (1960) suggested three different streamline patterns for a viscous liquid displaced by an inviscid fluid. For $m > 0.5$ there would be no flow reversion ahead of the bubble; for $m < 0.5$ one flow reversion ahead of the bubble would occur, with a stagnation point at the tip of the bubble and a stagnation ring right above it; and for $m = 0.5$ there would be flow reversion ahead of the bubble, but now showing two stagnation points: one at the tip of the bubble and the other a little far from the bubble, at the symmetry line.

In order to confirm Taylor's affirmatives, Goldsmith and Mason (1963) and Cox (1964) investigated experimentally the streamlines in front of the interface, and confirmed only two of the

patterns predicted by Taylor: the ones for $m < 0.5$ and $m > 0.5$. According to the last two authors' observations, these same streamline patterns are recovered in the present work simulations. Figures (3a) and (3b) show the streamlines ahead of the interface corresponding to the results obtained by Goldsmith and Mason and Cox.

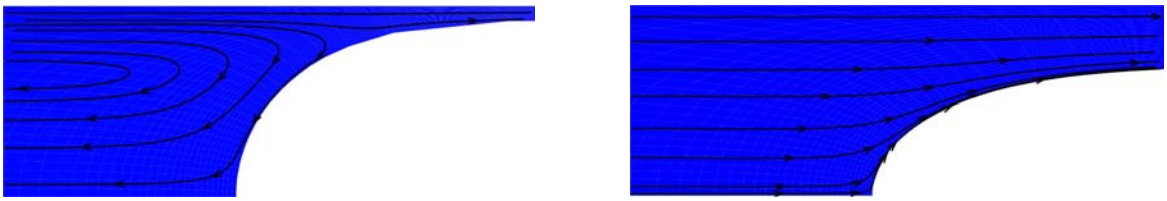

(a) (b)

Figure 3. Newtonian flow field as a function of *Ca*. Figure (3a) shows the streamlines for $Ca = 0.02$ ($m < 0.5$) and Fig. (3b) shows the streamlines for $Ca = 1.00$ ($m > 0.5$).

### 4.2. Viscoelastic Results

The evolution of the polymeric stress for the Oldroyd-B model as Deborah number rises is shown in Fig. (4).

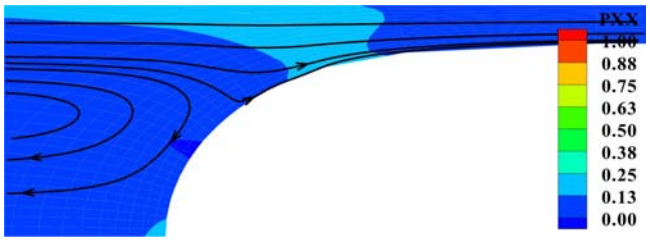


(a) $Ca = 0.10$ , $De = 0.50$

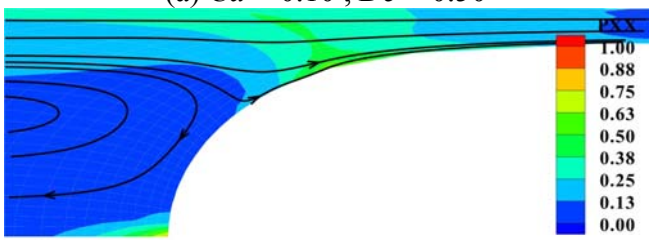


(b) $Ca = 0.10$ , $De = 1.00$

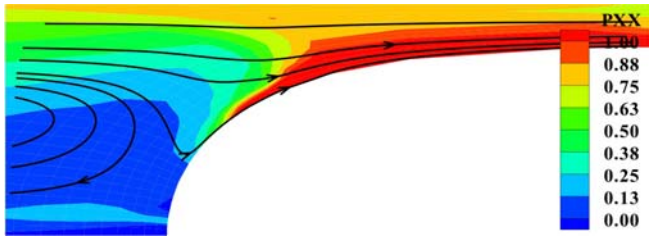


(c) $Ca = 0.10$ , $De = 3.00$

Figure 4. Polymer stress evolution as a function of *De*. The axial component of polymeric stress tensor field is shown in the background of figures (a), (b) and (c). Front lines represent streamlines. The flow states shown are at $Ca = 0.10$, but at all capillary numbers analyzed, a stress boundary layer appears attached to the free surface at high values of *De* (Fig. (4c)). Similar plots with the other components of the polymeric stress tensor were produced in order to study their contributions, but we have observed that the maximum stretch of the polymer molecules occurs downstream from the stagnation ring, i.e. the component of the stress tensor in the flow direction (shown here) is the most dominant in the flow. According to Lee et al. (2002), as shown in Fig. (4c), the maximum

polymeric stress is located downstream from the stagnation ring. Right after this point, a highly convergent flow is set in the region adjacent to the interface, and it appears that the stress boundary layer occurs due to the extension experienced by fluid elements in this region. An examination of the flow streamlines reveals that the contraction nature of the flow only affects fluid elements in the vicinity of the interface, while most of the streamlines remain rectilinear and parallel to the wall of the tube. This supports a mechanism proposed by Lee et al. (2002) that the extensional flow along the interface is responsible for the stress boundary layer formation.

Huzyak and Koelling (1997) performed experiments to investigate the penetration of a long bubble through a viscoelastic liquid in a capillary tube. In their work, the results were presented in terms of capillary number and Deborah number for four test fluids with rheological properties designed such that the effects of liquid elasticity could be isolated from shear thinning phenomena (Boger's fluids). In order to perform a comparison between their experimental data with our theoretical predictions, Fig. (5) shows an evolution of the ratio between the liquid film thickness obtained with a viscoelastic liquid (**m**) and that obtained with a Newtonian liquid at the same capillary number ($\mathbf{m_N}$) plotted against Deborah number. The experimental data corresponding to one of the viscoelastic liquids developed by Huzyak and Koelling (B-35), is compared with the theoretical predictions for an Oldroyd-B liquid for $Ca$ = 0.10. A value of reduced fractional coverage, $m/m_N$ = 1.0 implies that the amount of liquid attached to the wall when a viscoelastic liquid is displaced is the same as when a Newtonian liquid is displaced.

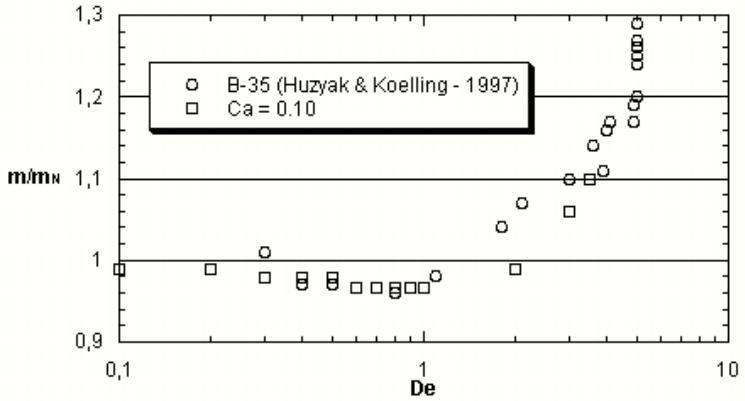


Figure 5. Reduced fractional coverage $m/m_N$ as a function of Deborah number. The circles correspond to experimental viscoelastic data obtained by Huzyak and Koelling, while the squares correspond to the present work numerical simulation data of an Oldroyd-B fluid for $Ca$ = 0.10.

The agreement between the experimental results of Huzyak and Koelling's and the theoretical predictions reported here is good. At small Deborah number, $De$ < 0.3, the reduced fractional coverage varies between $0.98 < \mathbf{m}/\mathbf{m_N} < 1.02$, indicating a Newtonian-like behavior. For $0.3 < De <$ 1, the film thickness at the wall when viscoelastic liquid is displaced is slightly thinner than the Newtonian case. At high Deborah numbers, $De$ > 1, the amount of liquid left on the capillary wall rises as the liquid becomes more viscoelastic. At $De$ = 3.5, it is 10% thicker than the Newtonian case.

The evolution of the stress field presented in Fig. (4) explains the thickening of the liquid film as Deborah number rises. As the liquid becomes more viscoelastic, the polymeric stress at the interface just downstream of the stagnation ring becomes higher. This high normal stress pulls the liquid and consequently moves the stagnation ring towards the bubble tip. This effect is clearly shown in Fig. (4c), where the streamline closest to the free surface is sharply bended towards the high normal stress region. As the stagnation rings moves upstream, the amount of liquid that turns around in the recirculation flow falls and consequently the deposited film thickness rises.

Figure (6) presents the predicted liquid film thickness at the capillary wall as a function of Deborah number at different capillary numbers. At small capillary numbers ($Ca$ = 0.05 and $Ca$ = 0.10) the behavior discussed in Figs. (4) and (5) is reproduced. At higher capillary numbers, the

ratio $\mathbf{m}/\mathbf{m_N}$ remains constant and equal to 1 up to $De \approx 1$. As Deborah number rises, the deposited film thickness increases. At a given Deborah number, the amount of film thickening falls as capillary number rises. An interesting observation that needs a more detailed analysis is that the film thickening due to elastic effects follows a logarithmic dependence on Deborah number.

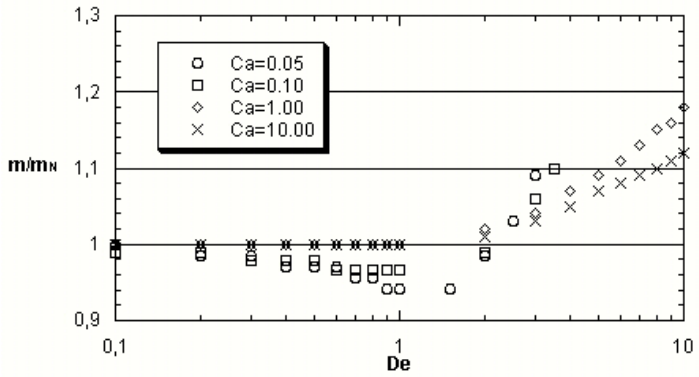


Figure 6. Evolution of reduced fractional coverage $m/m_N$ as a function of Deborah number for different capillary numbers.

## 5. FINAL COMMENTS

A two dimensional viscoelastic flow near the gas-liquid interface of a long bubble displacing a liquid in a capillary tube was presented. The presence of the free surface, that makes the domain of integration unknown a priori, and the differential constitutive model needed to describe the behavior of dilute polymeric solutions make the solution of the problem extremely complex. A fully coupled formulation was used and the differential equations were solved by the Finite Element Method.

The results show that viscoelastic forces tend to increase the amount of liquid left attached to the tube wall, a trend observed experimentally by other researchers. This work describes the mechanism responsible for this behavior.

## 6. ACKNOWLEDGEMENT

EFQ would like to thank CNPq for support through his doctor's degree scholarship.

## 7. REFERENCES

Benjamin, D.F., 1994, "Roll Coating Flows and Multiple Rolls Systems", PhD Thesis, University of Minnesota, Minneapolis, USA.

Bird, R.B., Armstrong, R.C. and Hassanger, O., 1987, "Dynamics of Polymeric Liquids, Vol. 1", 2nd ed., Wiley, New York, 649 p.

Bretherton, F.P., 1960, "The Motion of Long Bubbles in Tubes", J. of Fluid Mechanics, Vol. 10, pp. 166-188.

Brooks, A.N. and Hughes, T.J.R., 1982, "Streamline Upwind Petrov-Galerkin Formulations for Convection Dominated Flows with Particular Emphasis on the Incompressible Navier-Stokes Equations", Comput. Methods Appl. Mech. Eng., Vol. 32, pp. 199-259.

Cox, B.G., 1962, "On Driving a Viscous Fluid Out of a Tube", J. of Fluid Mechanics, Vol. 14, pp. 81-96.

Cox, B.G., 1964, "An Experimental Investigation of the Streamlines in Viscous Fluid Expelled from a Tube", J. of Fluid Mechanics, Vol. 20, pp. 193-200.

Fairbrother, F. and Stubbs, A.E., 1935, "Studies in Electroendosmosis. Part IV. The Bubble-Tube Method of Measurements", J. of Chemical Society, Vol. 1, pp. 527-529.

Goldsmith, H.L. and Mason, S.G., 1963, "The Flow of Suspensions Through Tubes II. Single Large Bubbles", J. Colloid Science, Vol. 18, pp. 237.

Guenette, R. and Fortin, M., 1995, “A New Mixed Finite Element Method for Computing Viscoelastic Flows”, J. Non-Newtonian Fluid Mechanics, Vol. 60, pp. 27-52.
Huzyak, P.C. and Koelling, K.W., 1997, “The Penetration of a Long Bubble Through a Viscoelastic Fluid in a Tube”, J. Non-Newtonian Fluid Mechanics, Vol. 71, pp. 73-88.
Lee, A.G., Shaqfeh, E.S.G. and Khomami, B., 2002, “A Study of Viscoelastic Free Surface Flows by the Finite Element Method: Hele-Shaw and Slot Coating Flows”, J. Non-Newtonian Fluid Mechanics, Vol. 108, pp. 327-362.
Pasquali, M. and Scriven, L.E., 2002, “Free Surface Flows of Polymer Solutions with Models Based on Conformation Tensor”, J. Non-Newtonian Fluid Mechanics, Vol. 108, pp. 363-409.
Ro, J.S. and Homsy, G.M., 1995, “Viscoelastic Free Surface Flows: Thin Film Hydrodynamics of Hele-Shaw and Dip Coating Flows”, J. Non-Newtonian Fluid Mechanics, Vol. 57, pp. 203-225.
Taylor, G.I., 1960, “Deposition of a Viscous Fluid on the Wall of a Tube”, J. of Fluid Mechanics, Vol. 10, pp. 161-165.